

Classical entanglement in polarization metrology

Falk Töppel^{1,2,3}, Andrea Aiello^{1,2}, Christoph Marquardt^{1,2},
Elisabeth Giacobino^{1,4} and Gerd Leuchs^{1,2}

E-mail: *falk.toeppel@mpl.mpg.de

¹ Max Planck Institute for the Science of Light, Günther-Scharowsky-Straße 1/Bldg. 24, 91058 Erlangen, Germany

² Institute for Optics, Information and Photonics, Universität Erlangen-Nürnberg, Staudtstraße 7/B2, 91058 Erlangen, Germany

³ Erlangen Graduate School in Advanced Optical Technologies (SAOT), Paul-Gordan-Straße 6, 91052 Erlangen, Germany

⁴ Laboratoire Kastler Brossel, Université Pierre et Marie Curie, Ecole Normale Supérieure, CNRS, 4 place Jussieu, 75252 Paris Cedex 05, France

Abstract. Quantum approaches relying on entangled photons have been recently proposed to increase the efficiency of optical measurements. We demonstrate here that, surprisingly, the use of classical light with entangled degrees of freedom can also bring outstanding advantages over conventional measurements in polarization metrology. Specifically, we show that radially polarized beams of light allow to perform real-time single-shot Mueller matrix polarimetry. Our results also indicate that quantum optical procedures requiring entanglement without nonlocality can be actually achieved in classical optics regime.

PACS numbers: 03.65.Ud, 41.20.-q, 42.25.Ja

1. Introduction

In the last years, quantum information theory taught us that the use of entangled photons offers the unique advantage over classical light of providing more information in metrology applications, imaging and, more generally, in optical measurements [1, 2, 3, 4, 5, 6]. However, entanglement is not necessarily a signature of the quantum mechanical nature of a system. Indeed, one can distinguish between two types of entanglement: *a*) entanglement between spatially separated systems (*inter*-system entanglement) and *b*) entanglement between different degrees of freedom (DoFs) of a single system (*intra*-system entanglement) [7, 8]. Inter-system entanglement, or “nonlocal entanglement”, can occur only in bona fide quantum systems and may yield to nonlocal statistical correlations. Conversely, intra-system entanglement, or “local entanglement”, may also appear in classical systems and can not generate nonlocal correlations [9]. As an example, photon pairs from atomic cascades [10] show nonlocal entanglement. On the opposite, local entanglement can be found, e.g., between spatial and spin DoFs in single neutrons [11]. In classical optics, local entanglement between polarization and spatial DoFs of the same beam, has been lately demonstrated in radially and azimuthally polarized beams of light [12, 13, 14, 15, 16, 17]. Hereafter, we shall denote the occurrence of local entanglement in classical systems with “classical entanglement” [8]‡.

Recently, Khoury and coworkers have suggested that quantum computing tasks requiring entanglement but not nonlocality can be efficiently accomplished in the classical optical regime [15]. However, when and how classical entanglement can be exploited in lieu of nonlocal entanglement to improve techniques of optical measurements, still remain largely open questions [21, 22, 23].

In this work, we address some of these central issues by proposing to use classical entanglement in radially polarized beams of light for highly efficient Mueller matrix polarimetry [24, 25, 26, 27]. The underlying idea is simple: In a conventional Mueller matrix measurement setting, an either transmissive or scattering material sample (the object) is illuminated with a light beam (the probe) prepared in, at least, *four* different polarization states in a temporal sequence. From the analysis of the polarization of the light transmitted or scattered, the optical properties of the object can be inferred. In the alternative setting we propose here, the object is probed only once with *one* light beam of radial polarization, as opposed to four differently polarized beams. Then, the light transmitted or reflected by the object is analyzed *both* in polarization and in spatial DoFs by means of suitable polarization and spatial mode selectors. In our setting, the polarization DoFs of the beam are used to actually probe the object and the spatial DoFs are used to postselect the polarization state of the light. This scheme outperforms conventional ones because the radially polarized beam carries all polarizations at once in a classically entangled state, thus providing for a sort of “polarization parallelism”.

‡ In the literature this phenomenon is also referred to as “structural inseparability” [18, 19] and “nonquantum entanglement” [20].

Hence, while with conventional Mueller matrix measurements it is necessary to probe the object fourfold, by using radially polarized light one can obtain the same amount of information by probing the sample only once. Therefore, for all practical applications where the optical properties of the sample changes rapidly with time, our method presents an outstanding advantage over conventional ones. We believe that this result can provide significant improvements in polarization metrology applications [24, 25, 28, 29, 30, 31, 32, 33]. Although our conclusions here are strictly valid only for optical elements that do not alter significantly the spatial structure of the probe beam, this is not a serious restriction. For example, all optical elements routinely used on an optical bench like single-mode fibers, retardation plates, birefringent prisms, optical rotators, etc., fall in this category. Moreover, our method can be also straightforwardly implemented by using less constrained entangled binary DoFs as, e.g., the polarization and spatial-parity modes considered by Saleh and coworkers [22, 34]. Another requirement for the validity of our scheme, is that the polarization properties of the sample must be homogeneous over the beam cross section. Considering that an ordinary radially polarized beam of light may be prepared with a waist of the order of hundreds of μm , such a requirement does not represent an actual limitation.

2. Jones vectors, entanglement and radially polarized beams

Consider a monochromatic beam of light of angular frequency ω , propagating along the z -axis of a Cartesian reference frame (x, y, z) and polarized in the (x, y) plane. In the paraxial approximation [35], the electric field can be written as $\mathcal{E}(\mathbf{r}, t) = \text{Re}[\mathbf{E}(\mathbf{r}) \exp(-i\omega t)]$, where

$$\mathbf{E}(\mathbf{r}) = (A_0 \mathbf{e}_x + A_1 \mathbf{e}_y) \psi(\mathbf{r}), \quad (1)$$

with $\psi(\mathbf{r})$ denoting the spatial mode of the beam, \mathbf{e}_x , \mathbf{e}_y and \mathbf{e}_z being unit vectors in the x , y and z directions, respectively. In the expression above, $\mathbf{r} = x\mathbf{e}_x + y\mathbf{e}_y + z\mathbf{e}_z$ stands for the position vector, and the two complex numbers A_0 and A_1 represent the amplitudes of the electric field along the x and y axis, respectively. A convenient vector notation for fields of the form (1) was introduced by R. C. Jones in the 1940s [25, 36]:

$$\mathbf{E}(\mathbf{r}) = \begin{bmatrix} A_0 \\ A_1 \end{bmatrix} \psi(\mathbf{r}). \quad (2)$$

With this notation, the identification of the polarization and the spatial DoFs, represented by the Jones vector $[A_0, A_1]^T$ and the scalar field $\psi(\mathbf{r})$, respectively, becomes straightforward.

For a field of the form (2), polarization and spatial DoFs are said to be *separable* [13] because the expression of $\mathbf{E}(\mathbf{r})$ is factorizable in the product of a single *space independent* vector, and a single scalar field. This mathematical property reflects the absence of physical coupling between polarization and spatial DoFs. However, in general, polarization and spatial DoFs can be coupled and when this happens the factorizable

representation (2) is no longer valid. Consider, for example, the electric field of a beam of light *nonuniformly* polarized in the (x, y) plane, which can be expressed as

$$\mathbf{E}(\mathbf{r}) = A_{00} \mathbf{e}_x \psi_{10}(\mathbf{r}) + A_{01} \mathbf{e}_x \psi_{01}(\mathbf{r}) + A_{10} \mathbf{e}_y \psi_{10}(\mathbf{r}) + A_{11} \mathbf{e}_y \psi_{01}(\mathbf{r}), \quad (3)$$

where $\psi_{mn}(\mathbf{r})$, with $m, n \in \{0, 1, 2, \dots\}$, is the Hermite-Gauss (HG) solution of the paraxial wave equation of order $N = m + n$ [35] and A_{ij} denotes a complex amplitude of the field, with $i, j \in \{0, 1\}$. In the Jones notation, (3) takes either of the two following forms:

$$\mathbf{E}(\mathbf{r}) = \begin{bmatrix} A_{00}\psi_{10}(\mathbf{r}) + A_{01}\psi_{01}(\mathbf{r}) \\ A_{10}\psi_{10}(\mathbf{r}) + A_{11}\psi_{01}(\mathbf{r}) \end{bmatrix} \quad (4a)$$

$$= \begin{bmatrix} A_{00} \\ A_{10} \end{bmatrix} \psi_{10}(\mathbf{r}) + \begin{bmatrix} A_{01} \\ A_{11} \end{bmatrix} \psi_{01}(\mathbf{r}). \quad (4b)$$

By writing the electric field as in (4a), it follows that the beam has a nonuniform polarization pattern because the Jones vector varies with the position vector \mathbf{r} . On the other hand, when $\mathbf{E}(\mathbf{r})$ is written in the form (4b), it appears evident that polarization and spatial DoFs are now *nonseparable*, or entangled, because one needs two coordinate-independent Jones vectors and two independent scalar fields, ψ_{10} and ψ_{01} ,[§] to represent the electric field.

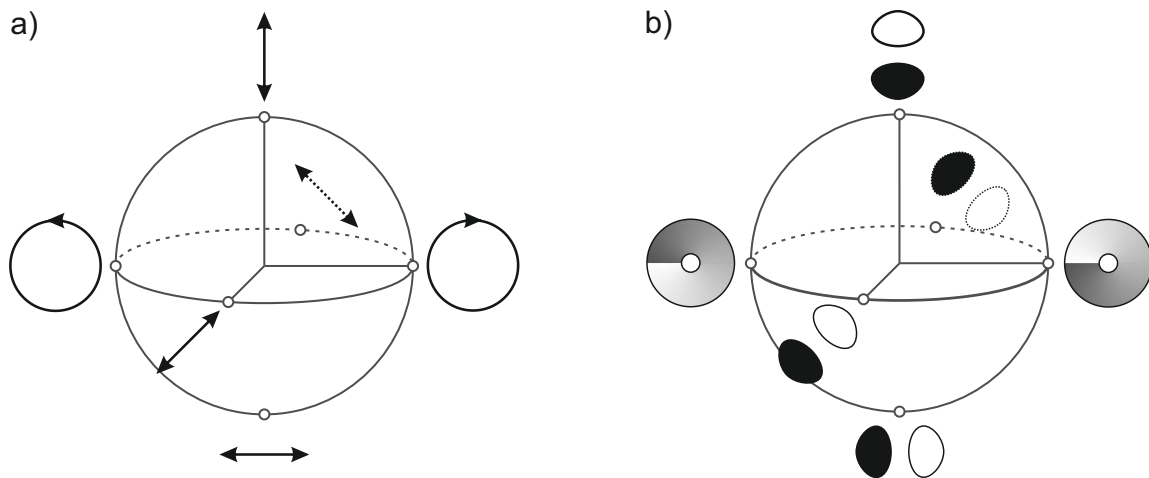


Figure 1. Schematic visualization of a) the polarization Poincaré sphere representation of the binary Hilbert space \mathcal{H}_{pol} [25] and b) Poincaré sphere representation of first-order spatial modes Hilbert space \mathcal{H}_{spa} [37].

Mathematically speaking, occurrence of entanglement requires an expression to be written as the sum of tensor products of two or more vectors belonging to different vector spaces. This is precisely what occurs in (4b), where we have a polarization vector space and a spatial vector space, which can be represented by the polarization Poincaré

[§] The HG-modes $\psi_{mn}(\mathbf{r})$ are independent in the sense that they are orthonormal with respect to the spatial scalar product defined as $\iint \psi_{mn}^*(\mathbf{r}) \psi_{m'n'}(\mathbf{r}) dx dy = \delta_{mm'} \delta_{nn'}$, with $m, m', n, n' \in \{0, 1, 2, \dots\}$.

sphere [25] and the first-order spatial modes Poincaré sphere [37], respectively, shown in figure 1. This qualitative discussion may be made more quantitative by considering a radially polarized beam of light as a specific example that can be represented by (3),

$$\mathbf{E}(\mathbf{r}) = \frac{1}{\sqrt{2}} \left[\mathbf{e}_x \psi_{10}(\mathbf{r}) + \mathbf{e}_y \psi_{01}(\mathbf{r}) \right], \quad (5)$$

whose characteristics are illustrated in figure 2. One can obtain (5) from (3) by putting

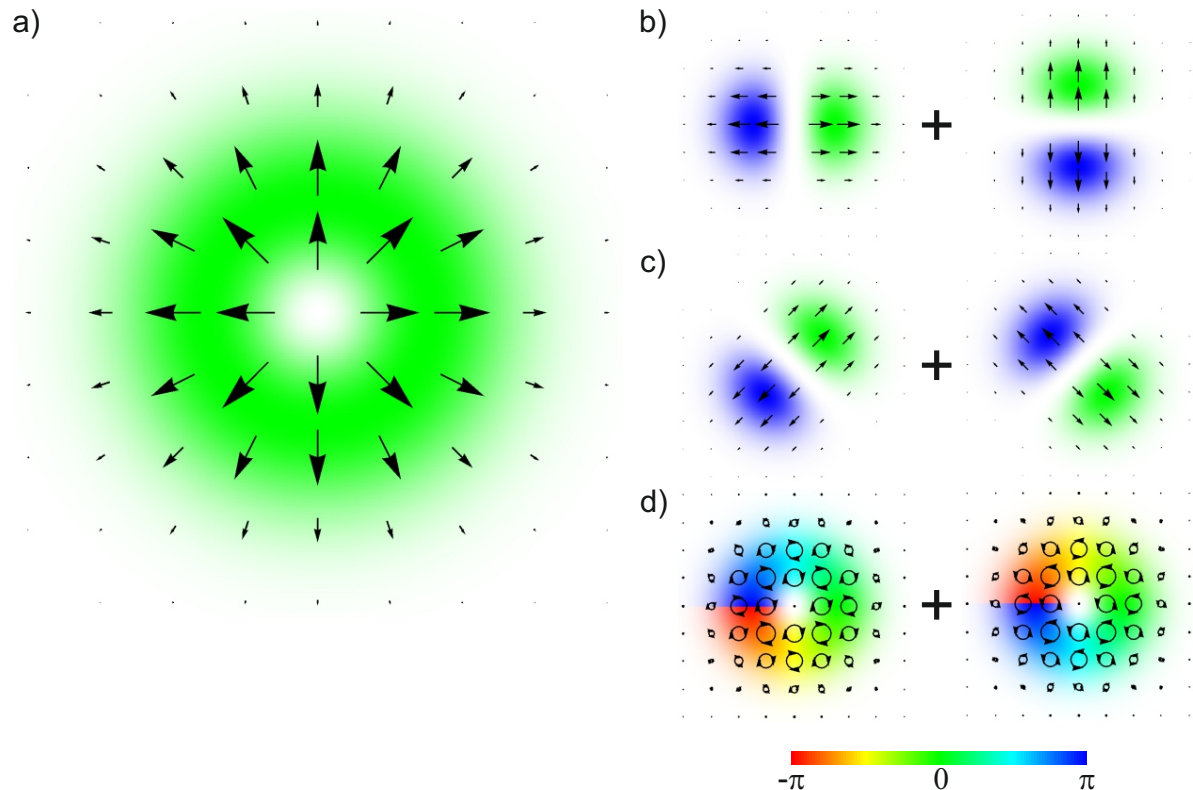


Figure 2. a) Visual representation of the intensity distribution and polarization pattern of the radially polarized beam of light (5). b - d) Possible equivalent decompositions of the beam (5): The color scale (bottom) gives the phase of the electric field. b) Superposing the electric fields of a HG mode ψ_{10} with horizontal polarization \mathbf{e}_x and a HG mode ψ_{01} with vertical polarization \mathbf{e}_y yields a radially polarized pattern: $\mathbf{E} = (\mathbf{e}_x \psi_{10} + \mathbf{e}_y \psi_{01})/\sqrt{2}$. c) Superposition of diagonal HG modes $\psi_{\pm} = (\psi_{10} \pm \psi_{01})/\sqrt{2}$ with diagonal polarizations $\mathbf{e}_{\pm} = (\mathbf{e}_x \pm \mathbf{e}_y)/\sqrt{2}$ also produces a radially polarized beam: $\mathbf{E} = (\mathbf{e}_+ \psi_+ + \mathbf{e}_- \psi_-)/\sqrt{2}$. d) Decomposition of a radially polarized beam into circular spatial modes $\psi_L = (\psi_{10} + i\psi_{01})/\sqrt{2}$, $\psi_R = (\psi_{10} - i\psi_{01})/\sqrt{2}$ and circular polarizations $\mathbf{e}_L = (\mathbf{e}_x + i\mathbf{e}_y)/\sqrt{2}$, $\mathbf{e}_R = (\mathbf{e}_x - i\mathbf{e}_y)/\sqrt{2}$ components: $\mathbf{E} = (\mathbf{e}_L \psi_R + \mathbf{e}_R \psi_L)/\sqrt{2}$.

$A_{00} = 1/\sqrt{2} = A_{11}$ and $A_{01} = 0 = A_{10}$. This suggests, as shown with great detail in [13, 18], that it is possible to represent a radially polarized beam by an abstract 4-dimensional vector, henceforth denoted with the ket $|E\rangle \doteq [A_{00}, A_{01}, A_{10}, A_{11}]^T$, living in a 4-dimensional two-qubit Hilbert space: $|E\rangle \in \mathcal{H}_2 = \mathcal{H}_{\text{pol}} \otimes \mathcal{H}_{\text{spa}}$. Here $\mathcal{H}_{\text{pol}} = \text{span}\{\mathbf{e}_x, \mathbf{e}_y\}$ denotes the polarization-qubit space and $\mathcal{H}_{\text{spa}} = \text{span}\{\psi_{10}(\mathbf{r}), \psi_{01}(\mathbf{r})\}$ indicates the spatial-qubit space. We identify the standard basis for the polarization

qubit with horizontal and vertical polarization states, and the standard basis for the spatial qubit with HG modes of order $n + m = 1$, namely

$$|0\rangle_{\text{pol}} := \mathbf{e}_x, \quad |1\rangle_{\text{pol}} := \mathbf{e}_y, \quad (6a)$$

$$|0\rangle_{\text{spa}} := \psi_{10}(\mathbf{r}), \quad |1\rangle_{\text{spa}} := \psi_{01}(\mathbf{r}). \quad (6b)$$

We can write a complete orthonormal basis of \mathcal{H}_2 in the form of a tensor product: $|i, j\rangle = |i\rangle_{\text{pol}} \otimes |j\rangle_{\text{spa}}$ with $i, j \in \{0, 1\}$, where the first index i marks the polarization qubit and the second index j the spatial one, namely

$$\begin{aligned} |0, 0\rangle &:= \mathbf{e}_x \psi_{10}(\mathbf{r}), & |0, 1\rangle &:= \mathbf{e}_x \psi_{01}(\mathbf{r}), \\ |1, 0\rangle &:= \mathbf{e}_y \psi_{10}(\mathbf{r}), & |1, 1\rangle &:= \mathbf{e}_y \psi_{01}(\mathbf{r}). \end{aligned} \quad (7)$$

With this notation we can represent the electric field (3) as a vector in \mathcal{H}_2 :

$$|E\rangle = A_{00} |0, 0\rangle + A_{01} |0, 1\rangle + A_{10} |1, 0\rangle + A_{11} |1, 1\rangle, \quad (8)$$

and a radially polarized beam can be described by the ket

$$|E\rangle = \frac{1}{\sqrt{2}} (|0, 0\rangle + |1, 1\rangle). \quad (9)$$

This representation for the radially polarized beam is formally equivalent (isomorphic) to a Bell state of two qubits [38]. Hence, the polarization and spatial DoF may be treated as two qubits that are classically entangled. However, the key difference between (9) and a bona fide quantum optical Bell state is that in the latter the two qubits are encoded in the polarization DoFs of *two* separated photons (inter-system entanglement), while in (9) the two qubits are encoded in the polarization and the spatial binary DoFs of a *single* light beam (intra-system entanglement).

3. Stokes parameters and the Liouville representation of a quantum state

The representations (3) and (8) for the electric field of a light beam are adequate as long as one is concerned with detection schemes that can resolve *both* polarization and spatial DoFs. When this is not the case, as in the conventional Mueller matrix polarimetry, it becomes necessary to introduce a more general representation, namely the 4×4 coherency matrix ρ of the field, defined in terms of the electric field amplitudes A_{ij} as

$$|E\rangle\langle E| := \rho = \begin{bmatrix} A_{00}A_{00}^* & A_{00}A_{01}^* & A_{00}A_{10}^* & A_{00}A_{11}^* \\ A_{01}A_{00}^* & A_{01}A_{01}^* & A_{01}A_{10}^* & A_{01}A_{11}^* \\ A_{10}A_{00}^* & A_{10}A_{01}^* & A_{10}A_{10}^* & A_{10}A_{11}^* \\ A_{11}A_{00}^* & A_{11}A_{01}^* & A_{11}A_{10}^* & A_{11}A_{11}^* \end{bmatrix}. \quad (10)$$

Of course, at this stage (10) still contains the same amount of information as (8). As a specific example, the coherency matrix of the radially polarized beam (9) can be simply written as

$$\rho = \frac{1}{2} \begin{bmatrix} 1 & 0 & 0 & 1 \\ 0 & 0 & 0 & 0 \\ 0 & 0 & 0 & 0 \\ 1 & 0 & 0 & 1 \end{bmatrix}. \quad (11)$$

Suppose now to have a detection scheme that is not capable to resolve the spatial DoFs. In this case, (8) would furnish redundant information about the spatial DoFs that is not at our disposal. However, a proper representation of the beam can be then obtained from (10) by tracing out the unobservable spatial DoFs. In this manner one obtains the reduced 2×2 polarization coherency matrix ρ_{pol} that encodes all the available information about the polarization of the light beam, irrespective of the spatial DoFs:

$$\begin{aligned} \rho \rightarrow \rho_{\text{pol}} &= \text{tr}_{\text{spa}}(\rho) \\ &= \sum_{i=0}^1 \text{spa} \langle i | \rho | i \rangle_{\text{spa}} \\ &= AA^\dagger, \end{aligned} \quad (12)$$

where $\text{tr}_{\text{spa}}(\dots)$ denotes the trace with respect to the spatial DoFs and the spatial kets $|0\rangle_{\text{spa}}$ and $|1\rangle_{\text{spa}}$ are defined in (6b). Here

$$A = \begin{bmatrix} A_{00} & A_{01} \\ A_{10} & A_{11} \end{bmatrix}, \quad (13)$$

is a 2×2 matrix whose elements are the coefficients A_{ij} of the ket expansion (8). In a similar manner, one can calculate the reduced 2×2 spatial coherency matrix ρ_{spa} that encodes all the available information about the spatial modes of the light beam, irrespective of the polarization:

$$\begin{aligned} \rho_{\text{spa}} &= \text{tr}_{\text{pol}}(\rho) \\ &= (A^\dagger A)^T, \end{aligned} \quad (14)$$

where $\text{tr}_{\text{pol}}(\dots)$ denotes the trace with respect to the polarization DoFs.

From the definition (12) it follows that ρ_{pol} is Hermitian and positive semidefinite. Therefore, it admits a Liouville representation of the form

$$\rho_{\text{pol}} = \frac{1}{2} \sum_{\mu=0}^3 S_\mu \sigma_\mu, \quad (15)$$

where the coefficients S_μ are real numbers and the set $\{\sigma_\mu\}_{\mu=0}^3$ of 2×2 Hermitean matrices forms a complete basis of observables [39]. The factor $1/2$ in front of (15) is conventional. In classical polarization optics, the coefficients S_μ are known as the Stokes parameters of the beam [40] and the basis set $\{\sigma_\mu\}_{\mu=0}^3$ is constituted by the four Pauli matrices

$$\begin{aligned} \sigma_0 &= \begin{bmatrix} 1 & 0 \\ 0 & 1 \end{bmatrix}, & \sigma_1 &= \begin{bmatrix} 0 & 1 \\ 1 & 0 \end{bmatrix}, \\ \sigma_2 &= \begin{bmatrix} 0 & -i \\ i & 0 \end{bmatrix}, & \sigma_3 &= \begin{bmatrix} 1 & 0 \\ 0 & -1 \end{bmatrix}, \end{aligned} \quad (16)$$

which are orthogonal with respect to the scalar product defined as $\text{tr}(\sigma_\mu \sigma_\nu) = 2\delta_{\mu\nu}$. From this property and the definition (15) it follows that

$$S_\mu = \text{tr}(\rho_{\text{pol}} \sigma_\mu). \quad (17)$$

For the radially polarized beam (9), $A = \mathcal{I}_2/\sqrt{2}$ and $\rho_{\text{pol}} = \mathcal{I}_2/2 = \rho_{\text{spa}}$, where \mathcal{I}_2 denotes the 2×2 identity matrix. In the language of classical polarization optics, this means that the radially polarized beam is completely unpolarized: $\mathbf{S} = [S_0, S_1, S_2, S_3]^T = [1, 0, 0, 0]^T$. This observation may appear confusing because (4a) and figure 2 show that a radially polarized beam possesses a well defined *local*, i.e. defined in each point (x, y) of its transverse spatial profile, Jones vector given by

$$\mathbf{E}(\mathbf{r}) = \frac{1}{\sqrt{2}} \begin{bmatrix} \psi_{10}(\mathbf{r}) \\ \psi_{01}(\mathbf{r}) \end{bmatrix}. \quad (18)$$

However, ρ_{pol} is obtained from ρ after tracing out the spatial DoFs. From a physical point of view, this corresponds to measuring the *global* Stokes parameters of the beam, as a whole, with “bucket” detectors that integrate the intensity of light over all the cross section of the beam. A similar situation is encountered for photon-pairs in a Bell state: Although the polarization of the two-photon state is perfectly defined (pure state), each of the two photons, when observed separately, appears as completely unpolarized (mixed state) [41].

4. Mueller matrix polarimetry

Typically, in a conventional polarimetry setup, an either transmissive or scattering material sample (the object) is illuminated with a light beam (input beam) that, as a result of the interaction with the object, emerges transformed (output beam). In this section we will study how radially polarized beams transform under the action of a polarization-affecting optical element, having in mind the final goal of measuring the Mueller matrix of the latter. From a mathematical point of view, here we consider local linear transformations of the form $T_{\text{pol}} \otimes T_{\text{spa}}$, namely transformations that act on each DoF separately, where $T_d : \mathcal{H}_d \rightarrow \mathcal{H}_d$ with $d \in \{\text{pol}, \text{spa}\}$ is a 2×2 complex matrix known as Jones matrix in polarization optics. As in this work we are concerned with optical elements affecting polarization DoFs solely, henceforth we assume $T_{\text{spa}} = \mathcal{I}_2$, and we will omit the subscript “pol” in T_{pol} .

Under the action of T , the generic ket (8) transforms as

$$\begin{aligned} |E\rangle \rightarrow |E'\rangle &= (T \otimes \mathcal{I}_2) |E\rangle \\ &= \sum_{i,j=0}^1 A'_{ij} |i, j\rangle, \end{aligned} \quad (19)$$

with $A' := TA$. The transformation (19) links the amplitudes A_{ij} of the input beam to the amplitudes A'_{ij} of the output beam. However, in real-world experiments intensities, rather than amplitudes, are measured. Therefore, it becomes necessary to specify the type of intensity measurements actually performed upon the output beam. According to whether the detectors are or are not insensitive to the spatial DoFs of the beam, one deals with either (a) single-DoF polarimetry or (b) two-DoF polarimetry. Case (a) coincides with the conventional Mueller matrix polarimetry, while case (b) gives the novel detection scheme that we propose here. Let us shortly review case (a) first.

4.1. Single-DoF polarimetry

From (19) and the definition (12) it follows that ρ_{pol} transforms under T as

$$\rho_{\text{pol}} \rightarrow \rho'_{\text{pol}} = A'A'^{\dagger} = TAA^{\dagger}T^{\dagger}. \quad (20)$$

Suppose we prepare sequentially the input beam in four different polarization states labeled by the index $\alpha \in \{0, 1, 2, 3\}$. For example, $\alpha = 0$ may denote horizontal polarization, $\alpha = 1$ vertical polarization, $\alpha = 2$ diagonal polarization and $\alpha = 3$ left-circular polarization. Then, in the Liouville representation (15) and by using the definition (17), the transformation (20) can be written, for each different input beam labeled by the index α , as

$$S'_{\mu}(\alpha) = \sum_{\nu=0}^3 M_{\mu\nu} S_{\nu}(\alpha), \quad \mu, \alpha \in \{0, 1, 2, 3\}, \quad (21)$$

where $S_{\nu}(\alpha)$ and $S'_{\mu}(\alpha)$ denote the Stokes parameters of the input and output beams, respectively, and the 16 real numbers

$$M_{\mu\nu} = \frac{1}{2} \text{tr}(\sigma_{\mu} T \sigma_{\nu} T^{\dagger}), \quad (22)$$

are the (unknown) elements of the sought Mueller matrix M .^{||} Then, (21) may be seen as a linear system of 16 equations and 16 unknowns that can be easily solved, for example, by defining the two 4×4 matrices V and V' as: $[V]_{\nu\alpha} := S_{\nu}(\alpha)$ and $[V']_{\mu\alpha} := S'_{\mu}(\alpha)$. This permits to rewrite (21) in the simple matrix form $V' = MV$, and the Mueller matrix M can be finally evaluated as

$$M = V'V^{-1}, \quad (23)$$

providing that $\det(V) \neq 0$.

This is the essence of conventional Mueller matrix polarimetry [42]. Of course, in a situation where experimental errors may occur, the simple linear inversion algorithm (23) often does not suffice and more sophisticated inversion methods must be used instead [26, 27]. However, the lesson to be learned here is that conventional Mueller matrix polarimetry needs the input beam to be sequentially prepared in, at least, four different polarization states to gain the complete information about the object. Conversely, we are going to show soon how the same amount of information can be obtained by probing the object only once with a radially polarized beam.

4.2. Two-DoF polarimetry

We now consider a detection scheme that is capable to resolve *both* the polarization and the spatial DoFs. The complete coherency matrix (10) can also be written in a Liouville

^{||} When the object is a depolarizing optical element, then (22) must be replaced with $M_{\mu\nu} = \overline{\text{tr}(\sigma_{\mu} T \sigma_{\nu} T^{\dagger})}/2$, where the overline symbol denotes average over a stochastic set [25]. For the sake of clarity, in the remainder we will consider only non-depolarizing optical elements.

form similar to (15) as

$$\rho = \frac{1}{4} \sum_{\mu, \nu=0}^3 S_{\mu\nu} (\sigma_\mu \otimes \sigma_\nu), \quad (24)$$

where we have defined the two-DoFs Stokes parameters as \P

$$S_{\mu\nu} = \text{tr}[\rho(\sigma_\mu \otimes \sigma_\nu)]. \quad (25)$$

These quantities are the classical optics analogue of the two-photon Stokes parameters introduced in [43, 44]. However, while in [44] the two polarization qubits are encoded in two *separated* photons, in our case the polarization qubit and the spatial qubit are encoded in the *same* radially polarized beam of light. Therefore, the two-DoFs Stokes parameters give the *intrabeam* correlations between polarization and spatial DoFs [45]. In order to measure these correlations, one needs a detection scheme capable to resolve both DoFs. Such an experimental apparatus will be studied in the next section. For the radially polarized beam represented by (11), the two-DoFs Stokes parameters take the particularly simple form

$$S_{\mu\nu} = \lambda_\mu \delta_{\mu\nu}, \quad \text{where} \quad \{\lambda_\mu\}_{\mu=0}^3 = \{1, 1, -1, 1\}. \quad (26)$$

From (19) it follows that, under the action of T , (11) transforms as

$$\begin{aligned} \rho \rightarrow \rho' &= (T \otimes \mathcal{I}_2) \rho (T^\dagger \otimes \mathcal{I}_2) \\ &= \frac{1}{4} \sum_{\mu=0}^3 \lambda_\mu (T \sigma_\mu T^\dagger) \otimes \sigma_\mu. \end{aligned} \quad (27)$$

Substituting (27) into (25) yields

$$\begin{aligned} S'_{\mu\nu} &= \text{tr}[\rho'(\sigma_\mu \otimes \sigma_\nu)] \\ &= \frac{1}{4} \sum_{\alpha=0}^3 \lambda_\alpha \text{tr}(\sigma_\mu T \sigma_\alpha T^\dagger) \text{tr}(\sigma_\alpha \sigma_\nu) \\ &= M_{\mu\nu} \lambda_\nu, \end{aligned} \quad (28)$$

where (22) has been used in the last line. Since either $\lambda_\nu = 1$ for $\nu \in \{0, 1, 3\}$ or $\lambda_\nu = -1$ for $\nu = 2$, from (28) it follows that the two-DoF Stokes parameters furnish a direct measure of the Mueller matrix elements:

$$M_{\mu\nu} = \begin{cases} -S'_{\mu\nu}, & \text{for } \nu = 2, \\ S'_{\mu\nu}, & \text{for } \nu \neq 2. \end{cases} \quad (29)$$

This shows that the Mueller matrix of an object can be obtained from the measurement of the 16 two-DoFs Stokes parameters $S'_{\mu\nu}$, with a single radially polarized input beam, allowing to perform single-shot full polarimetry. We remark that the above derivation relies upon the assumption that the optical properties of the object do not vary over the cross section of the input beam, namely that T is independent of x and y .

\P Here we are using the standard properties of the direct product of matrices: $(A \otimes B)(C \otimes D) = AC \otimes BD$ and $\text{tr}(A \otimes B) = \text{tr}(A) \text{tr}(B)$.

This interesting result can be understood as an effect of postselection on an entangled state. In a single-DoF polarimetry setup, the polarization state of the input beam is *preselected* before the interaction with the object, as shown in (21). Consequently, the object can be probed by only a single polarization state at a time. Vice versa, in our two-DoF polarimetry scheme the polarization state of the input beam is *postselected* after the interaction with the object via the two-DoF correlations measurements. Therefore, the object is probed, at once, by all possible polarization states carried by the radially polarized beam. This magic is made possible by the entangled structure (5) or (9) of the beam: projecting the output beam on a specific spatial mode uniquely determines, a posteriori, the polarization of the input beam, which may be either linear, diagonal or circular as shown in figure 2.

5. Real-time single-shot Mueller matrix polarimetry

In this section we propose a feasible experimental scheme for real-time single-shot Mueller matrix polarimetry. The measurement setup is illustrated in figures 3-5. The procedure we present here is an extension of the conventional polarization measurement technique to beams of light with coupled polarization and spatial DoFs. According to (29), the fundamental quantities to estimate are the sixteen two-DoF Stokes parameters $S_{\mu\nu}$ that contain all the information about the Mueller matrix.

The procedure is as follows: a radially polarized beam of light (the probe) is sent through a material sample (the object) whose Mueller matrix has to be determined. Then, the idea is to first project the beam transmitted across the sample onto the four independent spatial modes $\{\psi_{10}, \psi_{01}, \psi_+, \psi_-\}$ (also denoted with $\{\psi_0, \psi_1, \psi_2, \psi_3\}$).⁺ These projections postselect the four independent polarization states $\{e_x, e_y, e_+, e_-\}$, as explained in detail in subsection 5.1. It is important to stress that we perform these operations without acting directly on the polarization DoFs, which are analyzed only in a subsequent stage. For this, the light transmitted by the sample is split in three identical beams of equal intensity, which then are sent to mode converters (MCs) and mode beam splitters (MBSs). The three MCs, denoted as A, B and C in figure 3, define in which basis (ψ_L, ψ_R) , (ψ_+, ψ_-) or (ψ_{10}, ψ_{01}) the incoming beam is going to be measured. MC A that transforms the modes (ψ_L, ψ_R) into (ψ_{10}, ψ_{01}) , is made of a $\pi/2$ -converter, rotated by the angle $\theta = \pi/4$ with respect to the horizontal axis (see Appendix A). MC B, which transforms the modes (ψ_+, ψ_-) into (ψ_{10}, ψ_{01}) , is made of a π -converter, rotated by the angle $\theta = \pi/8$ with respect to the horizontal axis (see Appendix A). MC C is made of empty space and does not change the modes. It can be shown [46] that a π -MC can be physically realized with two identical cylindrical lenses separated by a distance $2f$ equal to two focal lengths ($2f$ CL), as shown in figure 4 a). Similarly,

⁺ Diagonal/antidiagonal spatial modes are defined as $\psi_{\pm} = (\psi_{10} \pm \psi_{01})/\sqrt{2}$ and left/right-circular spatial modes are written as $\psi_L = (\psi_{10} + i\psi_{01})/\sqrt{2}$ and $\psi_R = (\psi_{10} - i\psi_{01})/\sqrt{2}$, respectively. Similarly, diagonal/antidiagonal polarization states are defined as $e_{\pm} = (e_x \pm e_y)/\sqrt{2}$ and left/right-circular polarization ones as $e_L = (e_x + ie_y)/\sqrt{2}$ and $e_R = (e_x - ie_y)/\sqrt{2}$, respectively.

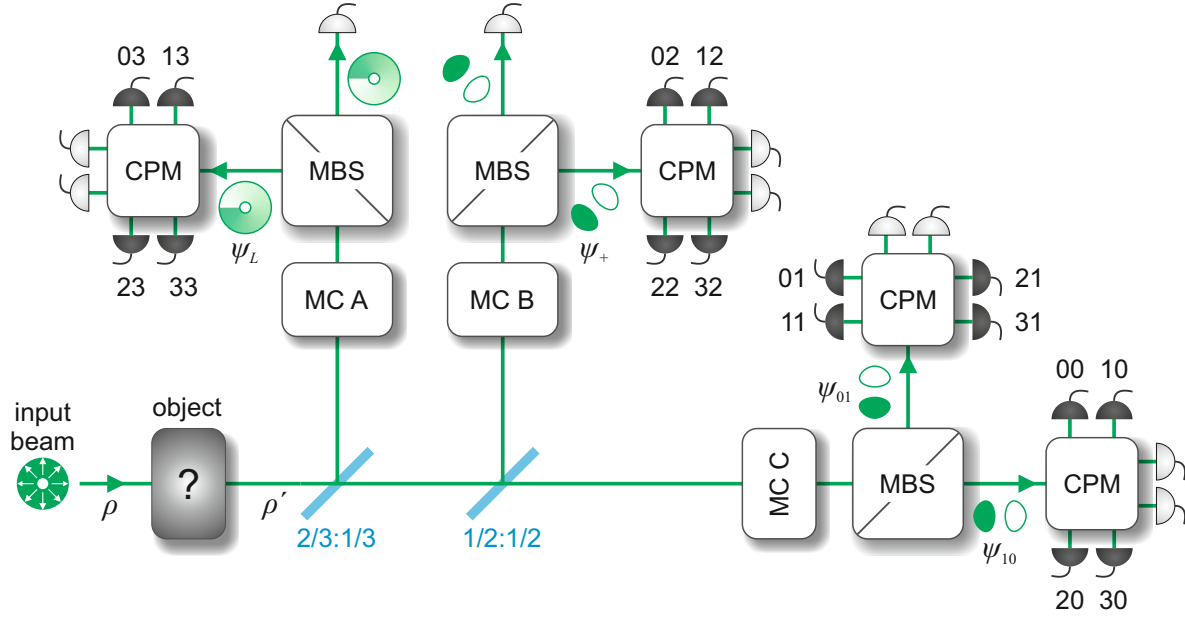


Figure 3. Schematic setup for real-time single-shot Mueller matrix polarimetry. The radially polarized input beam ρ propagates through a material sample (object) whose Mueller matrix must be determined. The light ρ' transmitted by the sample is split by polarization maintaining beam splitters (BSs) in three identical beams and sent through mode converters (MCs) followed by mode beam splitters (MBSs). The ratios of transmission (t) and reflection (r) coefficients of the BSs $|t|^2 : |r|^2$ are indicated in the figure. Each combination of a MC with a MBS effectively projects the entering beam on the specific spatial mode represented schematically in the figure. These operations postselect the polarization of the input beam as explained in the text. The four output ports of the three MBSs projecting onto the spatial modes $\{\psi_{10}, \psi_{01}, \psi_+, \psi_L\}$ (also denoted with $\{\psi_0, \psi_1, \psi_2, \psi_3\}$), are coupled to four distinct conventional polarization measurement setups (CPMs). Each CPM delivers the intensities of the four polarization components $\{e_x, e_y, e_+, e_L\}$ (also denoted with $\{e_0, e_1, e_2, e_3\}$), per each of the four entering beams $\psi_{10}, \psi_{01}, \psi_+$ or ψ_L . The detectors labeled with the polarization-spatial indexes $\alpha\beta$ with $\alpha, \beta \in \{0, 1, 2, 3\}$ in the figure, return the $4 \times 4 = 16$ intensities $I_{\alpha\beta}$, where, for example, $I_{10} = \langle e_y, \psi_{10} | \rho' | e_y, \psi_{10} \rangle$. From these intensities the two-DoF Stokes parameters $S_{\mu\nu}$ and the Mueller matrix can be completely determined via (1.13) and (29). In a setup that suffers from experimental imperfections, the intensities obtained by the 10 additional detectors displayed in light gray may be needed. Physical implementations of the MCs, MBS and CPM are shown in figures 4 and 5.

a $\pi/2$ -MC is made from two identical cylindrical lenses separated by a distance $\sqrt{2}f$ ($\sqrt{2}f$ CL), as illustrated in figure 4b). Each MC is coupled to a mode beam splitter (MBS), which splits up a beam into its ψ_{10} and ψ_{01} spatial components. The MBS is made of a modified Mach-Zehnder interferometer (MZ) with an extra mirror in one arm and a half-wave plate (HWP) in the other arm, followed by another HWP in one output port, as shown in figure 4 d) (see Appendix B and [47, 48]). As a result of these transformations, the MBS placed behind MC A splits up the incoming beam into its

circular spatial components, ψ_L and ψ_R , MC B splits the beam into its diagonal and antidiagonal spatial components ψ_+ and ψ_- and MC C into the ψ_{10} and ψ_{01} components. By selecting one of the outputs of MBS A and of MBS B and the two outputs of MBS C, one has access to the four spatial modes $\{\psi_{10}, \psi_{01}, \psi_+, \psi_L\}$. With this operation, we have physically acted only upon the spatial modes of the beam, and we will now analyze their polarization. This corresponds to a postselection of the polarization state of the probe beam. This is possible thanks to the entanglement between the polarization and the spatial DoFs.

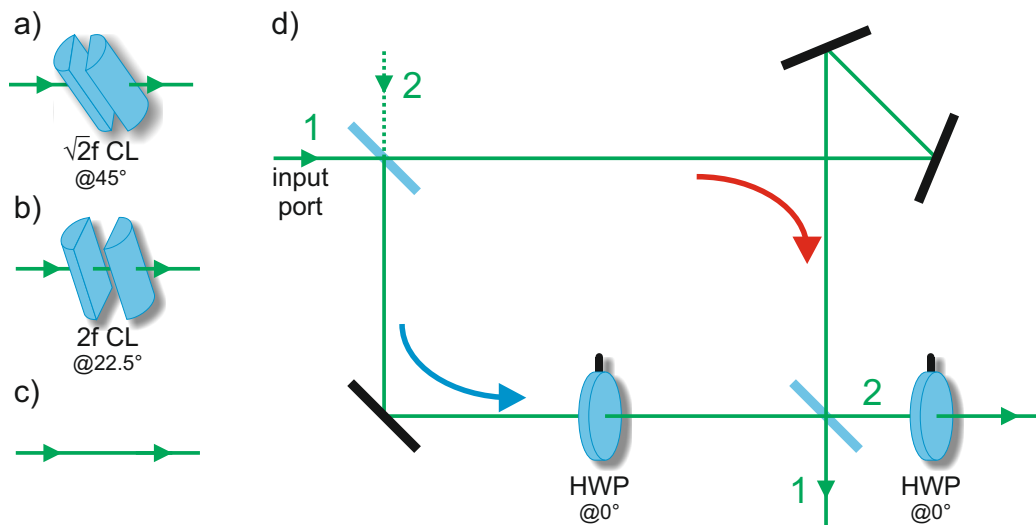


Figure 4. Physical implementation of mode converters (MCs) and the mode beam splitter (MBS) used in figure 3. a) MC A comprises a pair of identical cylindrical lenses at a distance of $\sqrt{2}f$ rotated by 45° with respect to the x -axis. b) MC B consists of a pair of identical cylindrical lenses separated by twice their focal length f and oriented at an angle of 22.5° with respect to the x -axis. c) MC C contains no optical elements. d) The MBS is realized with a Mach-Zehnder interferometer with an additional mirror in one arm and an additional half-wave plate (HWP) in the other arm with its fast axis oriented along the direction of horizontal polarization. The output port 2 of the interferometer is coupled to another HWP oriented identically to the first one. The presence of the second HWP becomes important when the MBS is coupled to a CPM.

The light exiting an output port of each MBS can be either directly detected, or sent through a conventional polarization measurement (CPM) setup shown in figure 5. A beam entering the CPM is split into three beams of equal intensity. Each beam passes through a polarization converter (PC) denoted with A, B and C in figure 3. They are made from, respectively, a) a quarter-wave plate (QWP) whose fast axis is tilted by $\pi/4$ with respect to the horizontal direction; b) a HWP with the fast axis rotated by $\pi/8$ with respect to the horizontal direction; and c) empty space. Each PC is coupled to a polarizing beam splitter (PBS), which splits a beam into its horizontal e_x and vertical e_y polarization components. The three combinations A, B and C of PCs and PBSs project the entering beams onto three mutually unbiased pairs of polarization states, namely, a) horizontal/vertical: $\{e_x, e_y\}$; b) diagonal/antidiagonal: $\{e_+, e_-\}$; and c)

left/right-circular: $\{\mathbf{e}_L, \mathbf{e}_R\}$, respectively. The intensity $I_{\alpha\beta}$ of the light projected in the state $\mathbf{e}_\alpha\psi_\beta$ is recorded by a photo-detector that is identified with the same pair of indexes $\alpha\beta : \alpha, \beta \in \{0, \dots, 3\}$. Here the first index α marks the polarization qubit and the second index β the spatial one, as shown in figure 1. When four independent spatial

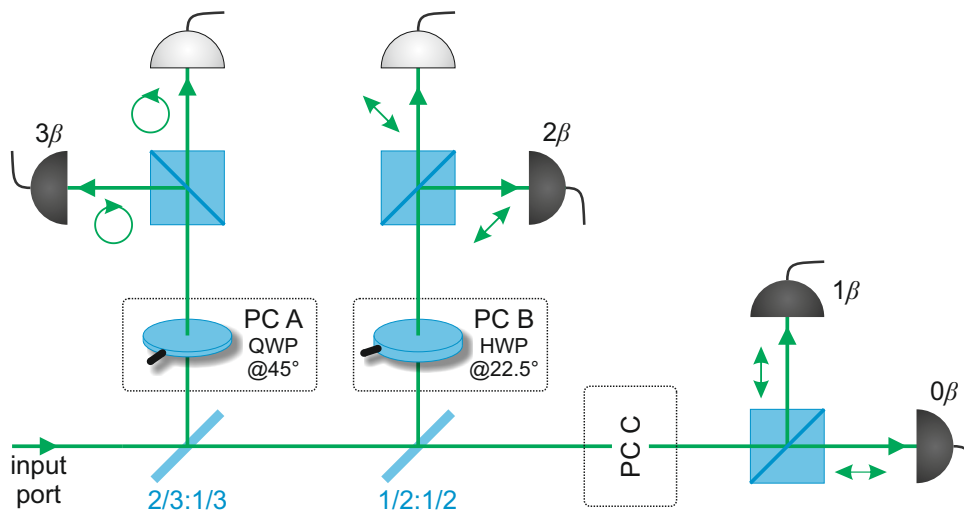


Figure 5. Physical implementation of the conventional polarization measurement setups (CPMs) used in figure 3. The input beam is split into three identical beams by two polarization maintaining beam splitters. Each of the three beams passes through a polarization converter (PC) followed by an polarizing beam splitter (PBS). PC A and PC B consist of a quarter-wave plate (QWP) and a half-wave plate (HWP), respectively. PC C is made from empty space. Complete information on the polarization state of the beam entering the input port can, in principle, be inferred from the measurements delivered by the 4 detectors labeled by the polarization-spatial indexes $\{0\beta, 1\beta, 2\beta, 3\beta\}$, where $\beta \in \{0, \dots, 3\}$ is the spatial mode index. However, in an experimental realization with unavoidable losses, the intensities measured by the 2 additional detectors displayed in light gray may be needed.

modes are sorted $\{\psi_{10}, \psi_{01}, \psi_+, \psi_L\} \equiv \{\psi_0, \psi_1, \psi_2, \psi_3\}$ by proper combinations of MCs and MBSs, and four independent polarization states $\{\mathbf{e}_x, \mathbf{e}_y, \mathbf{e}_+, \mathbf{e}_L\} \equiv \{\mathbf{e}_0, \mathbf{e}_1, \mathbf{e}_2, \mathbf{e}_3\}$ are selected by convenient sequences of PCs and PBSs, then the sixteen two-DoF Stokes parameters $S_{\mu\nu}$ can be entirely determined. In an ideal situation, the minimal number of detectors needed for this measurement is clearly 16. However, in real-world experiments where uncontrollable losses may occur, a maximal amount of 10 additional detectors may be used to ensure proper normalization of all measured quantities. It should be noticed that also in conventional Mueller matrix polarimetry at least 16 independent intensity measurements are required. The major advantage in our scheme is that we can perform the 16 measurements at the same time, thus providing a “real-time”, and potentially fast, Mueller matrix determination.

5.1. Determining the two-DoF Stokes parameters

In the remainder of this section, we will illustrate explicitly the two-DoF Stokes parameters measurement process putting particular emphasis into the postselection technique. For the sake of clarity, we will consider only the case of non-depolarizing (unknown) transmitting objects. More information about single- and two-qubit operations can be found in Appendix A.

The radially polarized input beam (9) can be represented by

$$|E\rangle = \frac{1}{\sqrt{2}} (|\mathbf{e}_x\rangle |\psi_{10}\rangle + |\mathbf{e}_y\rangle |\psi_{01}\rangle), \quad (30)$$

where the two-qubit basis (7) has been recast here in a more suggestive form. After interacting with the object, characterized by the (unknown) Jones matrix T , the state of the input beam is transformed according to:

$$|E\rangle \xrightarrow{T} |E'\rangle = \frac{1}{\sqrt{2}} \left[(T|\mathbf{e}_x\rangle) |\psi_{10}\rangle + (T|\mathbf{e}_y\rangle) |\psi_{01}\rangle \right]. \quad (31)$$

Using the decompositions of a radially polarized beam shown in figure 2, the state $|E'\rangle$ of the transmitted beam can be also written in the diagonal and circular mode bases as:

$$|E'\rangle = \frac{1}{\sqrt{2}} \left[(T|\mathbf{e}_+\rangle) |\psi_+\rangle + (T|\mathbf{e}_-\rangle) |\psi_-\rangle \right] \quad (32a)$$

$$= \frac{1}{\sqrt{2}} \left[(T|\mathbf{e}_L\rangle) |\psi_R\rangle + (T|\mathbf{e}_R\rangle) |\psi_L\rangle \right]. \quad (32b)$$

The three combinations of MCs and MBSs project the state $|E'\rangle$ onto the four independent modes ψ_{10} , ψ_{01} , ψ_+ , ψ_L . These are two-step operations: first a MC transforms the state $|E'\rangle$ into a chosen basis, then a MBS projects the transformed state onto the “linear” basis $\{\psi_{10}, \psi_{01}\}$. For example, from (1.5) and (32a) it follows that the transformation performed by MC B (first step) produces

$$\text{MC B} \longrightarrow U_\pi(\pi/8) |E'\rangle = \frac{-i}{\sqrt{2}} \left[(T|\mathbf{e}_+\rangle) |\psi_{10}\rangle + (T|\mathbf{e}_-\rangle) |\psi_{01}\rangle \right]. \quad (33)$$

Then, in the second step the MBS projects the state onto ψ_{01} and the result is:

$$\text{MBS} \longrightarrow \langle \psi_{01} | U_\pi(\pi/8) |E'\rangle = \frac{-i}{\sqrt{2}} T |\mathbf{e}_-\rangle. \quad (34)$$

These projections provide postselection of the four input polarization states \mathbf{e}_x , \mathbf{e}_y , \mathbf{e}_+ , \mathbf{e}_R , according to

$$\langle \psi_{10} | E'\rangle = \frac{1}{\sqrt{2}} T |\mathbf{e}_x\rangle, \quad (35a)$$

$$\langle \psi_{01} | E'\rangle = \frac{1}{\sqrt{2}} T |\mathbf{e}_y\rangle, \quad (35b)$$

$$\langle \psi_+ | E'\rangle = \frac{1}{\sqrt{2}} T |\mathbf{e}_-\rangle, \quad (35c)$$

$$\langle \psi_L | E'\rangle = \frac{1}{\sqrt{2}} T |\mathbf{e}_R\rangle, \quad (35d)$$

where irrelevant overall phase factors have been omitted. The states (35a-35d) exiting four different ports of the three MBSs, are then analyzed by CPMs that allow to evaluate all the elements of the Jones matrix T . Consider, for example, (35a). When this state is sent through a CPM, the following intensities can be measured:*

$$I_{00} \equiv |\langle \mathbf{e}_x | \langle \psi_{10} | E' \rangle|^2 = \frac{1}{2} |\langle \mathbf{e}_x | T | \mathbf{e}_x \rangle|^2, \quad (36a)$$

$$I_{10} \equiv |\langle \mathbf{e}_y | \langle \psi_{10} | E' \rangle|^2 = \frac{1}{2} |\langle \mathbf{e}_y | T | \mathbf{e}_x \rangle|^2, \quad (36b)$$

$$I_{20} \equiv |\langle \mathbf{e}_+ | \langle \psi_{10} | E' \rangle|^2 = \frac{1}{2} |\langle \mathbf{e}_+ | T | \mathbf{e}_x \rangle|^2, \quad (36c)$$

$$I_{30} \equiv |\langle \mathbf{e}_L | \langle \psi_{10} | E' \rangle|^2 = \frac{1}{2} |\langle \mathbf{e}_L | T | \mathbf{e}_x \rangle|^2. \quad (36d)$$

When the 16 intensities $I_{\alpha\beta}$ are measured, eventually the 16 two-DoF Stokes parameters $S_{\mu\nu}$ can be determined according to the formulas (1.13) given in Appendix A.2.

6. Conclusions

In this work we have shown how to exploit classical entanglement in polarization metrology, by using radially polarized beams of classical light to perform real-time single-shot Mueller matrix measurements. Our main result is that the Mueller matrix elements are simply proportional to the two-DoF Stokes parameters that quantify the intrabeam correlations between polarization and spatial DoFs of a radially polarized beam. The novelty of our approach is that while the speed of conventional Mueller matrix measurements is limited by the need of probing the sample four times *in sequence* with light of different polarization, in our setting the four probes are made *in parallel* via a single radially polarized beam of light. In conclusion, we have established a novel two-DoF polarimetry scheme, which is the classical wave analogue of two-photon polarimetry [44]. Our results generalise and extend to the classical optics regime some already known techniques of quantum metrology [4, 49, 50]. Last but not least, our work furnishes a clear proof of principle that optical measurements requiring entanglement but not nonlocality may be accomplished by using classical light.

Appendix A. Qubit operations

Appendix A.1. Single-DoF operations

Consider the single-qubit two-dimensional Hilbert space $\mathcal{H}_1 = \text{span}\{|0\rangle, |1\rangle\}$, where the standard basis states $|0\rangle$ and $|1\rangle$ are defined as the eigenstates of the σ_3 Pauli matrix in (16), irrespective of the specific DoF encoding the qubit. All the results obtained in this appendix are indeed equally valid for both polarization and spatial qubits, as defined

* As a technical remark, it should be noticed that the postselected set of polarization vectors $\{\mathbf{e}_x, \mathbf{e}_y, \mathbf{e}_+, \mathbf{e}_R\}$ does not coincide with the analyser basis $\{\mathbf{e}_x, \mathbf{e}_y, \mathbf{e}_+, \mathbf{e}_L\}$. However, this is not a problem as long as both set of vectors are linearly independent.

by (6a) and (6b). Similarly, the basis vectors $\{|+\rangle, |-\rangle\}$ and $\{|L\rangle, |R\rangle\}$ are defined as the eigenstates of the remaining two Pauli matrices σ_1 and σ_2 , respectively, where

$$|+\rangle = \frac{|0\rangle + |1\rangle}{\sqrt{2}}, \quad |-\rangle = \frac{|0\rangle - |1\rangle}{\sqrt{2}}, \quad (1.1a)$$

$$|L\rangle = \frac{|0\rangle + i|1\rangle}{\sqrt{2}}, \quad |R\rangle = \frac{|0\rangle - i|1\rangle}{\sqrt{2}}. \quad (1.1b)$$

Rotatable π - and $\pi/2$ -converters permit any transformation between these basis vectors [48]. According to [51], the unitary matrices representing π - and $\pi/2$ -converters can be written as:

$$U_\pi = e^{-i\pi/2} \begin{bmatrix} 1 & 0 \\ 0 & -1 \end{bmatrix}, \quad U_{\pi/2} = e^{-i\pi/4} \begin{bmatrix} 1 & 0 \\ 0 & i \end{bmatrix}, \quad (1.2)$$

where the conventional overall phase factors are fixed by the condition that, for the polarization qubit, the fast axis of both HWP and QWP are horizontal. The unitary matrix $U_\varphi(\theta)$, with $\varphi \in \{\pi, \pi/2\}$ for a φ -converter rotated by an angle θ , is given by

$$U_\varphi(\theta) = D(\theta) U_\varphi D(-\theta), \quad (1.3)$$

where $D(\theta)$ denotes the standard 2×2 rotation matrix:

$$D(\theta) = \begin{bmatrix} \cos \theta & -\sin \theta \\ \sin \theta & \cos \theta \end{bmatrix}. \quad (1.4)$$

For example, we can use (1.3) to transform the vectors (1.1a) and (1.1b) into the standard basis, as follows:

$$\begin{aligned} U_\pi(\pi/8)|+\rangle &= -i|0\rangle, & U_\pi(\pi/8)|-\rangle &= -i|1\rangle, \\ U_{\pi/2}(\pi/4)|L\rangle &= |0\rangle, & U_{\pi/2}(\pi/4)|R\rangle &= -i|1\rangle. \end{aligned} \quad (1.5)$$

Consider now the four basis states $\{|0\rangle, |1\rangle, |+\rangle, |L\rangle\}$ that we conveniently relabel as $\{|0\rangle, |1\rangle, |2\rangle, |3\rangle\}$. From these states we can build the four linearly independent projection matrices $E_\mu \equiv |\mu\rangle\langle\mu|$:

$$\begin{aligned} E_0 &= \begin{bmatrix} 1 & 0 \\ 0 & 0 \end{bmatrix} = \frac{\sigma_0 + \sigma_3}{2}, & E_1 &= \begin{bmatrix} 0 & 0 \\ 0 & 1 \end{bmatrix} = \frac{\sigma_0 - \sigma_3}{2}, \\ E_2 &= \begin{bmatrix} \frac{1}{2} & \frac{1}{2} \\ \frac{1}{2} & \frac{1}{2} \end{bmatrix} = \frac{\sigma_0 + \sigma_1}{2}, & E_3 &= \begin{bmatrix} \frac{1}{2} & \frac{-i}{2} \\ \frac{i}{2} & \frac{1}{2} \end{bmatrix} = \frac{\sigma_0 + \sigma_2}{2}. \end{aligned} \quad (1.6)$$

These relations can be inverted to give $\sigma_0 = E_0 + E_1$, $\sigma_1 = -E_0 - E_1 + 2E_2$, $\sigma_2 = -E_0 - E_1 + 2E_3$, $\sigma_3 = E_0 - E_1$ or, formally,

$$E_\mu = \sum_{\alpha=0}^3 g_{\mu\alpha} \sigma_\alpha, \quad \text{and} \quad \sigma_\mu = \sum_{\alpha=0}^3 f_{\mu\alpha} E_\alpha, \quad (\mu = 0, 1, 2, 3), \quad (1.7)$$

where, from the orthogonality of the Pauli matrices it follows that $g_{\mu\alpha} = \text{tr}(E_\mu \sigma_\alpha)/2$. The coefficients $f_{\mu\alpha}$ can be found by noticing that the two 4×4 matrices F and G defined as $[G]_{\mu\alpha} = g_{\mu\alpha}$ and $[F]_{\mu\alpha} = f_{\mu\alpha}$, are connected by the simple relation $F = G^{-1}$, which implies $f_{\mu\alpha} = [G^{-1}]_{\mu\alpha}$.

From an operational point of view, the projector E_2 can be physically implemented with a π -converter followed by the projector E_0 :

$$E_2 = U_\pi^\dagger(\pi/8) E_0 U_\pi(\pi/8), \quad (1.8)$$

where (1.5) has been used. Similarly, the projector E_3 can be realized with a $\pi/2$ -converter followed by the projector E_0 :

$$E_3 = U_{\pi/2}^\dagger(\pi/4) E_0 U_{\pi/2}(\pi/4). \quad (1.9)$$

Finally, the single-DoF Stokes parameters $S_\mu = \text{tr}(\rho_d \sigma_\mu)$, with ρ_d denoting the single-DoF 2×2 coherency matrix and $d \in \{\text{pol}, \text{spa}\}$, can be expressed in the basis $\{E_\alpha\}$ as

$$S_\mu = \sum_{\alpha=0}^3 f_{\mu\alpha} I_\alpha, \quad \text{where} \quad I_\alpha = \text{tr}(\rho_d E_\alpha). \quad (1.10)$$

For example, for polarization qubits I_α denotes the intensity of light polarized in the state $|\alpha\rangle$.

Appendix A.2. Two-DoF operations

The mathematical apparatus developed in Appendix A.1 can be used to express the two-DoF Stokes parameters $S_{\mu\nu}$ in terms of measurable intensities of light. To this end, it is enough to rewrite (25) in terms of the projection matrices $\{E_\mu\}$ as:

$$\begin{aligned} S_{\mu\nu} &= \text{tr}[\rho(\sigma_\mu \otimes \sigma_\nu)] \\ &= \sum_{\alpha, \beta=0}^3 f_{\mu\alpha} f_{\nu\beta} I_{\alpha\beta} \\ &= \sum_{\alpha, \beta=0}^3 (F \otimes F)_{\mu\nu, \alpha\beta} I_{\alpha\beta}, \end{aligned} \quad (1.11)$$

where $I_{\alpha\beta} \equiv \text{tr}[\rho(E_\alpha \otimes E_\beta)]$ denotes the intensity measured by the detector labeled by the pair of indexes α, β in figure 3, and (1.6) has been used for both the polarization and the spatial qubits. The last row of (1.11) furnishes a straightforward way to calculate the coefficients $f_{\mu\alpha} f_{\nu\beta}$. However, a more efficient formula can be obtained by defining the ‘‘intensity matrix’’ I via the relation $[I]_{\alpha\beta} = I_{\alpha\beta}$. Then, from (1.11) it follows that

$$S_{\mu\nu} = [F I F^T]_{\mu\nu}. \quad (1.12)$$

From (1.12) one obtains, for example, $S_{00} = I_{00} + I_{01} + I_{10} + I_{11}$ and $S_{31} = -I_{00} - I_{01} + 2I_{02} + I_{10} + I_{11} - 2I_{12}$. The expression for S_{00} originates directly from the relation $E_0 \otimes E_0 + E_0 \otimes E_1 + E_1 \otimes E_0 + E_1 \otimes E_1 = \mathcal{I}_4$, where \mathcal{I}_4 denotes the 4×4 identity matrix. A complete list of the two-DoF Stokes parameters $S_{\mu\nu}$ expressed in terms of the

intensities $I_{\alpha\beta}$ is given below:

$$\begin{aligned}
S_{00} &= I_{00} + I_{01} + I_{10} + I_{11}, \\
S_{01} &= -I_{00} - I_{01} + 2I_{02} - I_{10} - I_{11} + 2I_{12}, \\
S_{02} &= -I_{00} - I_{01} + 2I_{03} - I_{10} - I_{11} + 2I_{13}, \\
S_{03} &= I_{00} - I_{01} + I_{10} - I_{11}, \\
S_{10} &= -I_{00} - I_{01} - I_{10} - I_{11} + 2(I_{20} + I_{21}), \\
S_{11} &= I_{00} + I_{01} - 2I_{02} + I_{10} + I_{11} - 2(I_{12} + I_{20} + I_{21} - 2I_{22}), \\
S_{12} &= I_{00} + I_{01} - 2I_{03} + I_{10} + I_{11} - 2(I_{13} + I_{20} + I_{21} - 2I_{23}), \\
S_{13} &= -I_{00} + I_{01} - I_{10} + I_{11} + 2I_{20} - 2I_{21}, \\
S_{20} &= -I_{00} - I_{01} - I_{10} - I_{11} + 2(I_{30} + I_{31}), \\
S_{21} &= I_{00} + I_{01} - 2I_{02} + I_{10} + I_{11} - 2(I_{12} + I_{30} + I_{31} - 2I_{32}), \\
S_{22} &= I_{00} + I_{01} - 2I_{03} + I_{10} + I_{11} - 2(I_{13} + I_{30} + I_{31} - 2I_{33}), \\
S_{23} &= -I_{00} + I_{01} - I_{10} + I_{11} + 2I_{30} - 2I_{31}, \\
S_{30} &= I_{00} + I_{01} - I_{10} - I_{11}, \\
S_{31} &= -I_{00} - I_{01} + 2I_{02} + I_{10} + I_{11} - 2I_{12}, \\
S_{32} &= -I_{00} - I_{01} + 2I_{03} + I_{10} + I_{11} - 2I_{13}, \\
S_{33} &= I_{00} - I_{01} - I_{10} + I_{11}.
\end{aligned} \tag{1.13}$$

Appendix B. Mode beam splitter

We consider the experimental realization of a mode beam splitter (MBS) displayed in Fig. 4 d). To this end we use a right-handed coordinate system attached to the beam whose direction of propagation always coincides with the z -axis. On each reflection the handedness of the spatial modes is inverted and the phase difference between x and y -polarization components is shifted by π . This means that each reflection maps the coordinate x onto $-x$ and the polarization vector \mathbf{e}_x onto $-\mathbf{e}_x$. Hence, a mirror is described by the following transformation of the Jones vector:

$$\begin{bmatrix} E_x(\mathbf{r}) \\ E_y(\mathbf{r}) \end{bmatrix} \rightarrow i \begin{bmatrix} -E_x(\bar{\mathbf{r}}) \\ E_y(\bar{\mathbf{r}}) \end{bmatrix}, \tag{2.1}$$

where $\bar{\mathbf{r}} = -x\mathbf{e}_x + y\mathbf{e}_y + z\mathbf{e}_z$. Accordingly, a symmetric 50/50 beam splitter acts on the input field $[\mathbf{E}_1(\mathbf{r}), \mathbf{E}_2(\mathbf{r})]^T$ as follows:

$$\begin{bmatrix} E_{1x}(\mathbf{r}) \\ E_{1y}(\mathbf{r}) \\ E_{2x}(\mathbf{r}) \\ E_{2y}(\mathbf{r}) \end{bmatrix} \rightarrow \frac{1}{\sqrt{2}} \begin{bmatrix} E_{1x}(\mathbf{r}) - iE_{2x}(\bar{\mathbf{r}}) \\ E_{1y}(\mathbf{r}) + iE_{2y}(\bar{\mathbf{r}}) \\ E_{2x}(\mathbf{r}) - iE_{1x}(\bar{\mathbf{r}}) \\ E_{2y}(\mathbf{r}) + iE_{1y}(\bar{\mathbf{r}}) \end{bmatrix}, \tag{2.2}$$

where the subscripts 1 and 2 denote the two ports of the BS and, e. g., $\mathbf{E}_1(\mathbf{r})$ denotes the electric field of the beam entering port 1. The HWP with its fast optical axis aligned parallel to the horizontal direction is, according to (1.2), described by the transformation

$$\begin{bmatrix} E_x(\mathbf{r}) \\ E_y(\mathbf{r}) \end{bmatrix} \rightarrow i \begin{bmatrix} -E_x(\mathbf{r}) \\ E_y(\mathbf{r}) \end{bmatrix}. \tag{2.3}$$

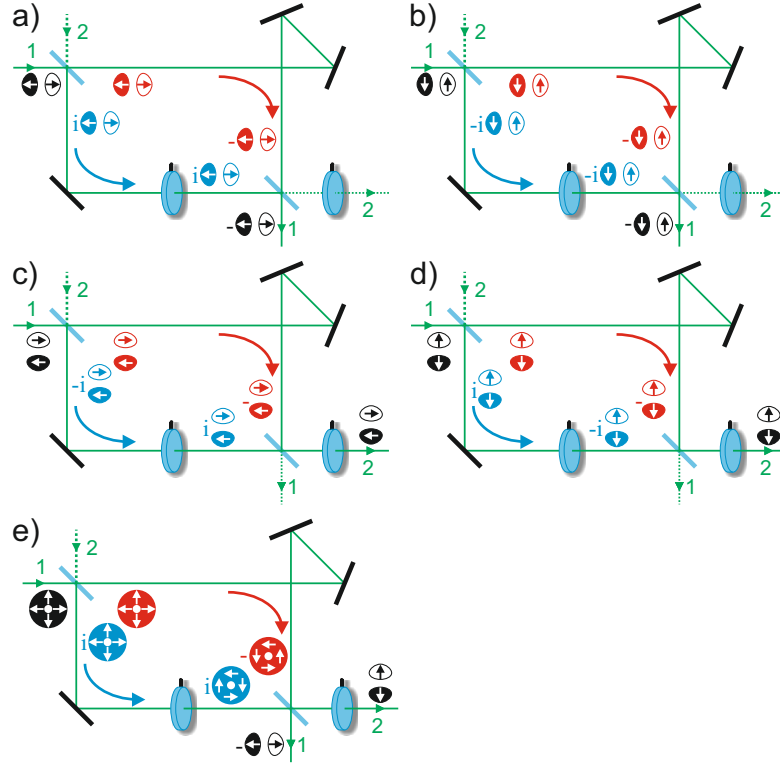


Figure B1. Visualization of the working principle of a mode beam splitter (MBS). The numbers 1 and 2 label the two arms of the MBS and dashed lines denote dark channels. a-b) The horizontally and vertically polarized HG modes $\mathbf{E}_1^{\text{in}}(\mathbf{r}) = \mathbf{e}_x \psi_{10}(\mathbf{r})$ and $\mathbf{E}_1^{\text{in}}(\mathbf{r}) = \mathbf{e}_y \psi_{10}(\mathbf{r})$ are transmitted across port 1. c-d) The horizontally and vertically polarized HG modes $\mathbf{E}_1^{\text{in}}(\mathbf{r}) = \mathbf{e}_x \psi_{01}(\mathbf{r})$ and $\mathbf{E}_1^{\text{in}}(\mathbf{r}) = \mathbf{e}_y \psi_{01}(\mathbf{r})$ are transmitted across port 2. e) The MBS splits a radially polarized beam $\mathbf{E}_1^{\text{in}}(\mathbf{r}) = [\mathbf{e}_x \psi_{10}(\mathbf{r}) + \mathbf{e}_y \psi_{01}(\mathbf{r})]/\sqrt{2}$ in its components $\mathbf{E}_1^{\text{out}}(\mathbf{r}) = \mathbf{e}_x \psi_{10}(\mathbf{r})$ and $\mathbf{E}_2^{\text{out}}(\mathbf{r}) = \mathbf{e}_y \psi_{01}(\mathbf{r})$.

As our proposal uses solely first-order spatial modes, let us consider the input fields $\mathbf{E}_1^{\text{in}}(\mathbf{r}) = [A_{00}\psi_{10}(\mathbf{r}) + A_{01}\psi_{01}(\mathbf{r})] \mathbf{e}_x + [A_{10}\psi_{10}(\mathbf{r}) + A_{11}\psi_{01}(\mathbf{r})] \mathbf{e}_y$ and $\mathbf{E}_2^{\text{in}}(\mathbf{r}) = \mathbf{0}$. The MBS transforms these input fields into the output fields

$$\mathbf{E}_1^{\text{out}}(\mathbf{r}) = -(A_{00}\mathbf{e}_x + A_{10}\mathbf{e}_y)\psi_{10}(\mathbf{r}), \quad (2.4)$$

and

$$\mathbf{E}_2^{\text{out}}(\mathbf{r}) = (A_{01}\mathbf{e}_x + A_{11}\mathbf{e}_y)\psi_{01}(\mathbf{r}). \quad (2.5)$$

as can be shown by successively applying the transformations of each element of the MBS described above. Furthermore, it was used the fact that the HG mode ψ_{10} changes sign upon reflection, i.e. $\psi_{10}(\bar{\mathbf{r}}) = -\psi_{10}(\mathbf{r})$, whereas this is not the case for the HG mode ψ_{01} , i.e. $\psi_{01}(\bar{\mathbf{r}}) = \psi_{01}(\mathbf{r})$.

References

- [1] Massar S and Popescu S 1995 Optimal Extraction of Information from Finite Quantum Ensembles *Phys. Rev. Lett.* **74**(8) 1259–63
- [2] Gisin M 2001 Coherent quantum measurement for the direct determination of the degree of polarization and polarization mode dispersion compensation *J. Mod. Opt.* **48**(8) 1397–403
- [3] Abouraddy A F, Saleh B E A, Sergienko A V, and Teich M C 2001 Role of entanglement in two-photon imaging *Phys. Rev. Lett.* **87**(12) 123602
- [4] Aiello A and Woerdman J P 2004 Linear Algebra for Mueller Calculus *Preprint* arXiv: 0412061 [math-ph]
- [5] Legré M, Wegmüller M and Gisin N 2003 Quantum Measurement of the Degree of Polarization of a Light Beam *Phys. Rev. Lett.* **91**(16) 167902
- [6] Brunner N, Acín A, Collins D, Gisin N and Scarani V 2003 Optical Telecom Networks as Weak Quantum Measurements with Postselection *Phys. Rev. Lett.* **91**(18) 180402
- [7] Gisin N 1991 Bells inequality holds for all non-product states *Phys. Lett.* **154**(5-6) 201–2
- [8] Spreuw, R J C 1998 A classical analogy of entanglement *Foundations of Physics* **28**(3) 361–74
- [9] Brunner N, Gisin N and Scarani V 2005 Entanglement and non-locality are different resources *New J. Phys.* **7**(1) 88
- [10] Aspect A 1983 Experimental Tests of Bell’s Inequalities in Atomic Physics *Atomics Physics* **8** 103–28
- [11] Hasegawa Y, Loidl R, Badurek G, Baron M, and Rauch H 2003 Violation of a Bell-like inequality in single-neutron interferometry *Nature* **425**(6953) 45–8
- [12] Souza C E R, Huguenin J A O, Milman P and Khoury A Z 2007 Topological Phase for Spin-Orbit Transformations on a Laser Beam *Phys. Rev. Lett.* **99**(16), 160401
- [13] Luis A 2009 Coherence, polarization, and entanglement for classical light fields *Opt. Commun.* **282**(18) 3665–70
- [14] Holleczek A, Aiello A, Gabriel C, Marquardt Ch and Leuchs G 2010 Poincarè sphere representation for classical inseparable Bell-like states of the electromagnetic field arXiv:1007.2528 [physics.optics]
- [15] Borges C V S, Hor-Meyll M, Huguenin J A O and Khoury A Z 2010 Bell-like inequality for the spin-orbit separability of a laser beam *Phys. Rev. A* **82**(3) 033833
- [16] Karimi E, et al. 2010 Spin-orbit hybrid entanglement of photons and quantum contextuality *Phys. Rev. A* **82**(2) 022115
- [17] Qian X-Feng and Eberly J H 2011 Entanglement and classical polarization states *Opt. Lett.* **36**(2) 4110–2
- [18] Holleczek A, Aiello A, Gabriel Ch, Marquardt Ch and Leuchs G 2011 Classical and quantum properties of cylindrically polarized states of light *Opt. Express* **19**(10) 9714–36
- [19] Gabriel Ch, et al 2011 Entangling Different Degrees of Freedom by Quadrature Squeezing Cylindrically Polarized Modes *Phys. Rev. Lett.* **106**(6) 060502
- [20] Simon B N, Simon S, Gori F, Santarsiero M, Borghi R, Mukunda N and Simon R 2010 Nonquantum Entanglement Resolves a Basic Issue in Polarization Optics *Phys. Rev. Lett.* **104**(2) 023901
- [21] de Oliveira A N , Walborn S P and Monken C H 2005 Implementing the Deutsch algorithm with polarization and transverse spatial modes *J. Opt. B: Quantum Semiclass. Opt.* **7**(9) 288–92
- [22] Kagalwala K H, Di Giuseppe G, Abouraddy A F and Saleh B E A 2013 Bell’s measure in classical optical coherence *Nat. Phot.* **7**(2) 72–8
- [23] Ghose P and Mukhrjee A 2014 Entanglement in Classical Optics *Reviews in Theoretical Science* **2**(4) 274–88
- [24] Mueller H 1943 Memorandum on the polarization optics of the photo-elastic Shutter *Report Number 2 of the OSRD Project OEMsr-576*
- [25] Damask J N 2005 *Polarization Optics in Telecommunications* (New York: Springer)
- [26] Le Roy-Brehonnet F and Jeune B L 1997 Utilization of Mueller matrix formalism to obtain optical

- targets depolarization and polarization properties *Prog. Quantum Electron.* **21**(2) 109–51.
- [27] Aiello A, Puentes G, Voigt D and Woerdman J P 2006 Maximum-likelihood estimation of Mueller matrices *Opt. Lett.* **31**(6) 817–9
- [28] Schieck H P gen 2012 *Nuclear Physics with Polarized Particles* (Lecture Notes in Physics, Vol. 842) (Springer-Verlag Berlin Heidelberg)
- [29] Clarke D 2010 *Stellar Polarimetry* (Wiley-VCH)
- [30] Van Zyl J J 2011 *Synthetic Aperture Radar Polarimetry* (JPL Space Science and Technology Series) (John Wiley & Sons, Inc., Hoboken, New Jersey)
- [31] Tuchin V V, Wang L, Zimnyakov D A 2006 *Optical Polarization in Biomedical Applications* (Springer-Verlag Berlin Heidelberg)
- [32] Schott J R 2009 *Fundamentals of Polarimetric Remote Sensing* (SPIE Tutorial Text Vol. TT81, SPIE Washington)
- [33] Firdous S 2010 *Laser tissue interaction and wave propagation in random media: Mueller matrix Polarimetry* (VDM Verlag)
- [34] Abouraddy A F, Yarnall T M, Di Giuseppe G, Teich M C and Saleh B E A 2012 Encoding arbitrary four-qubit states in the spatial parity of a photon pair *Phys. Rev. A* **85**(6) 062317
- [35] Siegman A E 1986 *Lasers* (Mill Valley: University Science Books) ch 16
- [36] Jones R C 1941 A new calculus for the treatment of optical systems, I. Description and Discussion of the Calculus *J. Opt. Soc. Am.* **31**(7) 488–93
- [37] Padgett M J and Courtial J 1999 Poincaré-sphere equivalent for light beams containing orbital angular momentum *Opt. Lett.* **24**(7) 430–2
- [38] Nielsen M A and Chuang I L 2010 *Quantum Computation and Quantum Information* (Cambridge: University Press Cambridge)
- [39] Balian R 1999 Incomplete descriptions and relevant entropies *Am. J. Phys.* **67**(12) 1078–90
- [40] Mandel L and Wolf E 1995 *Optical Coherence and Quantum Optics* (Cambridge: University Press Cambridge)
- [41] Lehner J, Leonhardt U and Paul H 1996 Unpolarized light: Classical and quantum states *Phys. Rev. A* **53**(4) 2727–35
- [42] Bickel W S and Bailey W M 1985 Stokes vectors, Mueller matrices, and polarized scattered light *Am. J. Phys.* **53**(5) 468–78
- [43] James D F V, Kwiat P G, Munro W J and White A G 2001 Measurement of qubits *Phys. Rev. A* **64**(5) 052312
- [44] Abouraddy A F, Sergienko A V, Saleh B E A, and Teich M C 2002 Quantum entanglement and the two-photon Stokes parameters *Opt. Commun.* **201**(1–3) 93–8
- [45] Loudon R 2001 *The Quantum Theory of Light* (Oxford: Oxford University Press, 3rd ed)
- [46] Beijersbergen M W, Allen L, van der Veen H E L O and Woerdman J P 1993 Astigmatic laser mode converters and transfer of orbital angular momentum *Opt. Commun.* **96**(1–3) 123–32
- [47] Sasada H and Okamoto M 2003 Transverse-mode beam splitter of a light beam and its application to quantum cryptography *Phys. Rev. A* **68**(1) 012323
- [48] Luda M A, Larotonda M A, Paz J P, Schmiegelow C T 2013 Manipulating Transverse Modes of Photons for Quantum Cryptography *Preprint* arXiv:1312.4365 [quant-ph]
- [49] Aiello A, Puentes G and Woerdman J P 2007 Linear optics and quantum maps *Phys. Rev. A* **76**(3) 032323
- [50] Toussaint K C, Di Giuseppe G, Bycenski K J, Sergienko A V, Saleh B E A and Teich M C 2004 Quantum ellipsometry using correlated-photon beams *Phys. Rev. A* **70**(2) 023801
- [51] Pedrotti F L and Pedrotti L S 1993 *Introduction to Optics* (Englewood Cliffs, NJ : Prentice-Hall) ch 14